# Endocytosis caused by liquid-liquid phase separation of proteins

Louis-Philippe Bergeron-Sandoval[1], Hossein Khadivi Heris[2], Adam G. Hendricks[2], Allen J. Ehrlicher[2], Paul François[3], Rohit V. Pappu[4] and Stephen W. Michnick[1,5*]

## Affiliations

[1]Département de Biochimie, Université de Montréal, C.P. 6128, Succursale centre-ville, Montréal, Québec, H3C 3J7, Canada.
[2]Department of Bioengineering, McGill University, Montreal, Quebec, H3A0C3, Canada.
[3]Ernest Rutherford Physics Building, 3600 rue University, McGill University, Montreal, Québec, H3A2T8
[4]Department of Biomedical Engineering and Center for Biological Systems Engineering, Washington University in St. Louis, One Brookings Drive, Campus Box 1097, St. Louis, Missouri 63130, USA.
[5]Centre Robert-Cedergren, Bio-Informatique et Génomique, Université de Montréal, C.P. 6128, Succursale centre-ville, Montréal, Québec, H3C 3J7, Canada.

*Correspondence to: S.W.M. (stephen.michnick@umontreal.ca).

## Summary

Clathrin-mediated endocytosis (CME) underlies intra- and extracellular material trafficking in eukaryotes, and is essential to protein metabolism, intercellular signaling, membrane remodeling and other cell regulatory processes. Although CME is usually driven by F-actin polymerization, membrane invagination can also occur through unknown actin independent mechanisms. Here, we present evidence that CME is driven by the accumulation of proteins at sites of endocytosis initiation that undergo liquid-liquid phase separation to form viscoelastic droplets. The surfaces of these droplets, bind to the membrane and surrounding cytosol and generate the work required to drive membrane invagination. The proposed mechanism expands the repertoire of functions of membraneless organelles that form via liquid-liquid phase separation to include their ability to do work due to soft interfaces that shape and organize cellular matter.

## Introduction

Evolution has resulted in numerous innovations by which morphogenesis of organisms occurs within limits imposed by physical and chemical constraints on the underlying biochemical processes (Darwin 1859, Thompson 1917). At the cellular level these biochemical processes include active polymerization of cytoskeletal proteins (Pollard and Cooper 2009), motor protein regulation of polymerization (Haviv, Gillo et al. 2008) and cytoplasmic transport (Hendricks, Holzbaur et al. 2012, Guo, Ehrlicher et al. 2014), the generation and maintenance of osmotic gradients (Meshcheryakov, Steudle et al. 1992) and peptidoglycan cell walls (Harold 1990). However, the mechanical forces that drive some subcellular mechanics remain a mystery. This includes the membrane invagination and vesicle formation process called clathrin-mediated endocytosis (CME) (Aghamohammadzadeh and Ayscough 2009, Boulant, Kural et al. 2011, Li, Shao et al. 2015). In the baker's yeast *Saccharomyces cerevisiae* CME is preceded by the spatially focused accumulation of a number of proteins on the plasma membrane, among which are those that encode low amino acid sequence complexity and structurally disordered "prion-like domains" (PLD) (Fig. 1a) (Kaksonen, Toret et al. 2005, Hom, Vora et al. 2007, Idrissi, Blasco et al. 2012, Malinovska, Kroschwald et al. 2013, Brach, Godlee et al. 2014, Avinoam, Schorb et al. 2015). Here, we demonstrate that membrane invagination can arise from liquid-liquid phase separation (demixing) of PLD-containing proteins from the cytosol. Demixing of these proteins results in formation of a droplet, which, by virtue of its viscoelastic properties, binds to and deforms plasma membrane and cytosol to which it binds. Demonstration that phase separated droplets can perform mechanical work expands the repertoire of known protein droplet functions to include the ability to do work at the droplet surfaces and their interfaces. Similar mechanisms may govern or contribute to other membrane shaping, invagination and budding processes that are involved in the cellular material uptake, secretion, and cell shape remodeling.

In *S. cerevisiae,* the dominant force for vesicle generation in CME is branched actin assembly, which is required to compete against intracellular turgor pressure and membrane tension to drive the invagination of the plasma membrane (Drubin, Kaksonen et al. 2005, Carlsson and Bayly 2014, Dmitrieff and Nedelec 2015, Li, Shao et al. 2015). If, however, turgor pressure is eliminated, CME in *S. cerevisiae* cells can also occur independent of actin polymerization (Aghamohammadzadeh and Ayscough 2009).

Alternative mechanisms to explain actin-independent membrane invagination in CME include intrinsic twisting of the membrane by the clathrin matrix, binding of curved BAR (Bin/Amphiphysin/Rvs) domain-containing proteins, protein domain insertion in the membrane bilayer, or steric repulsion of coat and adaptor proteins due to their crowding at cortical CME nucleation sites. Although these models are physically plausible, as demonstrated in model systems, their importance *in vivo* remain controversial (detailed in Material and Methods) (Carlsson and Bayly 2014, Kukulski, Picco et al. 2016, Scher-Zagier and Carlsson 2016). For instance, deletion of the only F-BAR domain-containing protein that accumulates on cortical

sites prior to excision, Syp1, does not affect membrane invagination (Fig. S1) (Boettner, D'Agostino et al. 2009).

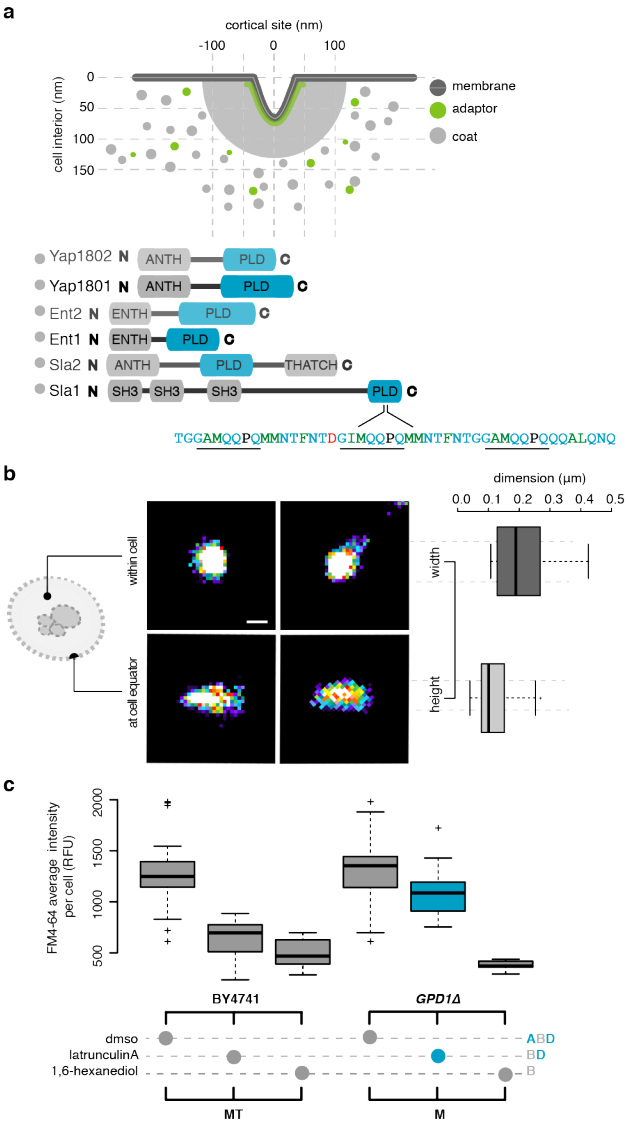


**Figure 1 | Assembly of proteins into a cortical droplet drive clathrin-mediated endocytosis** (a) (Upper panel) Illustration of the geometry of a plasma membrane (dark grey) invagination into the cell during clathrin-mediated endocytosis (CME). 70 nm invagination is required for vesicle scission to occur. Electron microscopic data suggest that clathrin-coated plasma membrane patches are surrounded by a cortical body of ~200 nm diameter (light grey) before appearance of actin structures. Clathrin heavy and light chains (Chc1 and Clc1) interact with adaptor proteins (Ede1 and Syp1) to form a lattice on the membrane (in green). Subsequently, early coat proteins (light grey), such as Sla1/2, Ent1/2, and Yap1801/2, directly bind to the adaptor-clathrin lattice and form the cortical body (in grey). (lower panel) Coat proteins contain "Prion-like domains" (PLD, in blue) that include tandem repeats of asparagine and glutamine. (b) Geometry and size distribution of coat protein Sla1-GFP at cortical sites measured using super-resolution microscopy (dSTORM). Lateral x, y resolution was ~10 nm. Pseudo-color reconstructed images show circular structures (left panels) when viewed from the top, or within cells (left, upper), but

form narrow ellipses when imaged at the equator of cells (left, lower). Automatic segmentation and morphological analysis (right) were performed on these reconstructed images to determine the width (209 ± 10 nm) and height (118 ± 6 nm) of cortical bodies (mean ± sd; n = 250), consistent with other electron and light micrographic evidence. (c) Lipophilic cargo membrane-labelling dye FM4-64 is taken up into vesicles by CME in wild type (left) and *GPD1*Δ cells (eliminates turgor pressure; right) treated with either DMSO, latrunculin A (prevents F-actin polymerization) or 1,6-hexanediol (disrupts liquid-liquid phase separated protein droplets). Each boxplot shows the relative fluorescence units of n = 50 cells. Note that *GPD1*Δ cells can undergo CME in the absence of F-actin polymerization (blue) because there is no turgor pressure in these cells (Fig. S2-3).

A potential mechanism that could drive actin-independent CME in yeast was suggested to us by the observation that there is a common amino acid sequence pattern found among coat and adapter proteins. Several of these proteins have PLDs (Fig. 1a) (Alberti, Halfmann et al. 2009, Malinovska, Kroschwald et al. 2013). Such proteins are known to phase separate *in vitro* and in cells to form spherical condensates or droplets that are hundreds of nanometers to micrometers in size and having a range of viscoelastic properties (Guilak, Tedrow et al. 2000, Pappu, Wang et al. 2008, Brangwynne, Eckmann et al. 2009, Hyman, Weber et al. 2014, Banjade, Wu et al. 2015, Jiang, Wang et al. 2015, Kroschwald, Maharana et al. 2015, Molliex, Temirov et al. 2015, Nott, Petsalaki et al. 2015, Zhang, Elbaum-Garfinkle et al. 2015). We postulate that such droplets exist at CME initiation sites and that, owing to their viscoelastic properties and interfacial tension bind to the plasma membrane adaptors and generate a force that drives invagination of the membrane (Hertz 1882, Johnson 1971, Ewers, Romer et al. 2010, Style, Hyland et al. 2013).

**PLD-containing CME proteins accumulate and phase separate at cortical sites**

Evidence that a protein droplet (henceforth called the cortical droplet) could form at CME sites include first, electron and light microscopic studies that reveal a region surrounding CME membrane invaginations and mature vesicles of ~200 nm diameter that is devoid of ribosomes (Kukulski, Schorb et al. 2012, Picco, Mund et al. 2015). This "exclusion zone" thus appears to present a physical barrier to large molecular complexes at least as large as ribosomes (> 10 nm) (Kukulski, Schorb et al. 2012). Furthermore, we and as others have observed an object at cortical sites of ~200 nm diameter by super-resolution imaging of Sla1 in cells treated with Latrunculin A (LatA), an inhibitor of actin polymerization. The exclusion zone cannot, thus, be attributed only to F-actin bundles (Fig. 1b, Fig. S4) (Picco, Mund et al. 2015). Our results agree with quantitative immuno-EM data which show that many endocytic coat proteins (including Sla1/2 and Ent1/2) assemble into a hemisphere of similar dimensions, consistent with a protein droplet that associates with membrane on cortical sites (Idrissi, Grotsch et al. 2008, Idrissi, Blasco et al. 2012).

The simple alcohol 1,6-hexanediol (HD) has been demonstrated to prevent liquid-liquid phase separation of proteins to form droplets *in vivo* and *in vitro* (Updike, Hachey et al. 2011, Kroschwald, Maharana et al. 2015, Molliex, Temirov et al. 2015, Wheeler, Matheny et al. 2016,

Rog, Kohler et al. 2017). CME, as measured by cell uptake of a lipophilic membrane-bound fluorescent dye (FM4-64), was inhibited by HD, whether or not turgor pressure and actin polymerization were present (Fig. 1c, left *versus* right panels, respectively). Furthermore, an HD dose-response of uptake of the fluorescent dye (Lucifer Yellow) into vacuoles and formation of puncta monitored as Sla1-GFP fluorescence at cortical sites were prevented, but not in cells treated with the related alcohol 1,2,3-Hexanetriol that does not disrupt droplets (Fig. 2a, Fig. S5). The other PLD-containing proteins, including Sla2, Ent1, Ent2, Yap1801 and Yap1802, all failed to form puncta in cells treated with HD (Fig. S5). Pulse-chase experiments showed that HD-dependent dissolution of Sla1 puncta was reversible (Fig. S6 and movie 1). Finally, PLD-containing proteins can also form amyloid aggregates, which can be diagnosed by binding and co-localization of Thioflavin T (ThT) to the aggregates (Khurana, Coleman et al. 2005). We observed no colocalization of ThT with Sla1-mCherry-labelled puncta (Fig. S7).

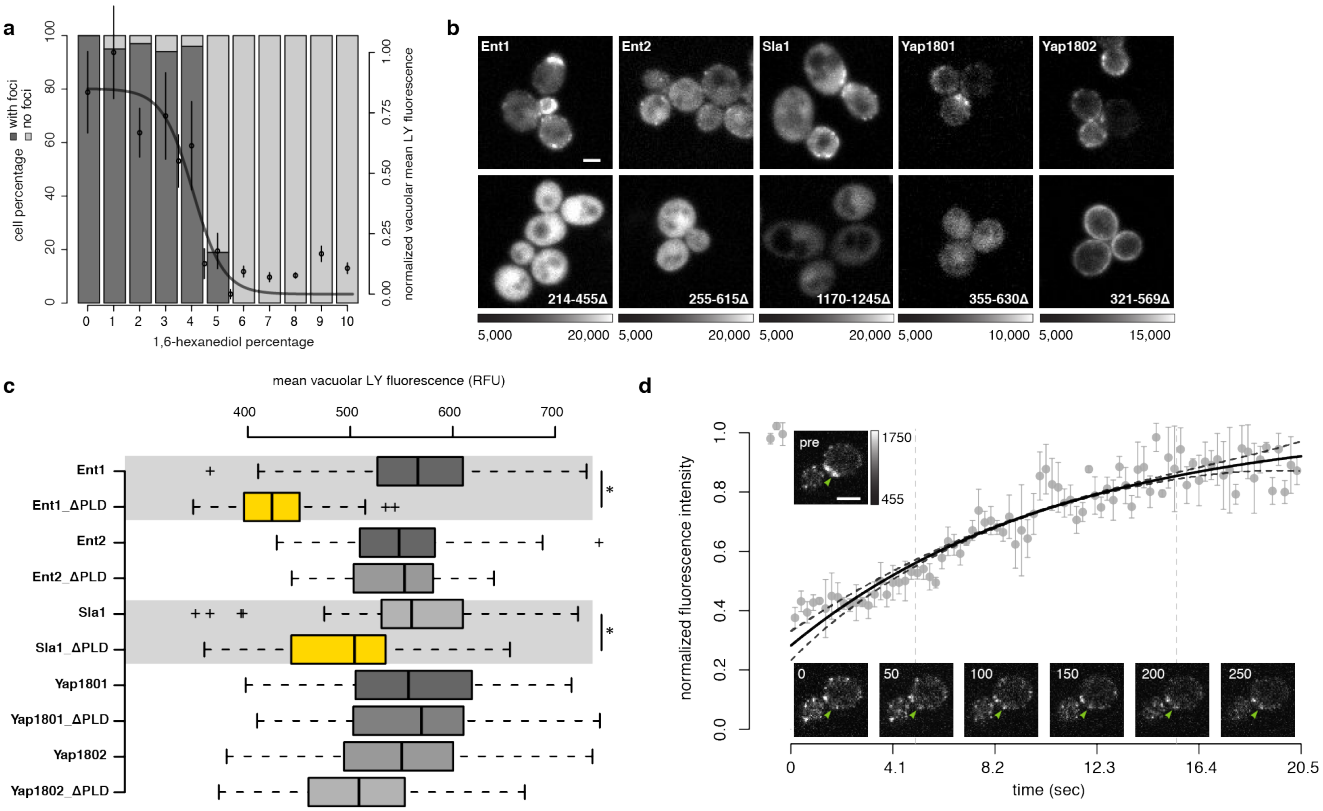


**Figure 2 | CME adaptor and coat proteins phase separate to form droplets** (a) 1,6-hexanediol (HD), disrupts cortical droplets in an all-or-none manner. Barplot shows percentage of cells that contain Sla1-GFP foci (dark grey), or not (light grey), as a function of HD concentration monitored by counting fluorescent puncta containing Sla1-GFP at cortical sites 5 minutes after HD treatment (n = 150 cells). Plot overlay (in black) shows quantification of lucifer yellow fluorescent dye uptake in CME vesicles (mean ± sd; n = 25; logistic fit) (b) Prion-like domains (PLDs) are essential for localization of proteins to the cortical sites. Fluorescence images of cortical localization of Ent1, Ent2, Sla1, Yap1801 and Yap1802 fused to Venus YFP. Localization of full-length (upper panels) *versus* C-terminal PLD truncation mutants of the proteins (lower panels). Amino acid positions of the deleted PLDs are indicated for respective

157 images. Grayscale dynamic range for image pairs are indicated below. Scale bar, 2 μm. (c) Quantification
158 by fluorescence microscopy of lucifer yellow dye uptake for strains that express either full-length or
159 PLD-truncated Ent1, Ent2, Yap1801, Yap1802 and Sla1 (as detailed in panel b). We observed a
160 significant decrease in CME for PLD truncation mutants of Sla1 and Ent1 (two-sided t-test; star indicates
161 $P < 0.001$; $n = 100$ cells). (d) Coat proteins exchange with cortical droplets at rates typical of those
162 observed for proteins that compose other protein droplets. Fluorescence recovery after photo bleaching
163 (FRAP) of Sla2-GFP, GFP signal recovery was measured within a segmented Sla1-mCherry region of
164 interest to ensure that FRAP was acquired within the cortical droplet (mean ± sd; $n = 5$); photo bleached
165 Sla1-mCherry region identified arrows in image inserts. Data was fitted to a single term recovery equation
166 (full line) and corrected for the known rate of molecule accumulation and depletion that occurs during the
167 droplet lifecycle (dashed lines) (Material and Methods). Incomplete fluorescence recovery suggests that
168 cortical droplets are viscoelastic. Representative cell images before bleaching, upon bleaching, and after
169 recovery are shown in inserts; frame numbers are indicated in the upper left of each image. Grayscale
170 values, 455 to 1750. Scale bar, 2 μm.
171
172 The PLDs of cortical CME proteins were essential to their localization to cortical sites (Fig. 2b).
173 Furthermore, CME was significantly reduced in cells where the PLDs of Sla1 and Ent1 were
174 deleted and with substitutions of proline for other residues in the Sla1 PLD, which weakens the
175 driving force for phase separation (Fig. 2c, Fig. S8) (Toombs, McCarty et al. 2009, Crick, Ruff et
176 al. 2013). Our results support evidence that there is a functional redundancy among most of the
177 PLD-containing proteins with the two that are more essential, perhaps required for specific
178 functions mediated by other domains within their sequences (Watson, Cope et al. 2001, Godlee
179 and Kaksonen 2013).
180
181 The interactions among proteins in liquid-liquid phase separated droplets are expected to be
182 weak and this is assessed by their rapid exchange within and between droplets and their
183 surroundings (Brangwynne, Eckmann et al. 2009, Elbaum-Garfinkle, Kim et al. 2015, Lin,
184 Protter et al. 2015, Feric, Vaidya et al. 2016). In fluorescence recovery after photobleaching
185 (FRAP) experiments we measured both mobile (0.7±0.2) and immobile (0.3±0.2) fractions for
186 the coat protein Sla2 and rapid recovery time (7.5 seconds), similar to other protein and nucleic
187 acid droplets including the dense internal fibrillar component of *X. laevis* nucleoli (Fig. 2d)
188 (Feric, Vaidya et al. 2016). Taken together, these results support the hypothesis that the cortical
189 bodies are phase separated viscoelastic droplets. We next set out to determine the material
190 properties of the cortical droplets and to test our postulate that their binding to the plasma
191 membrane generates the force that drives invagination of the membrane.
192
193 **Cortical droplets can mechanically deform both cytosol and membrane**
194
195 We hypothesized that free energy released by cortical droplet phase separation is converted into
196 mechanical work to deform the membrane and the cytosol. Simply stated, we posit that binding
197 of the droplet to cytosol draws the droplet inward as it grows, while the membrane follows,
198 mediated by its own binding to the droplet and the requirement that the volume of the droplet be
199 conserved. This idea is captured by the well-known Johnson-Kendall-Roberts (JKR) theory,

which describes how non-flat material surfaces stick to and conform to one another in order to minimize their interfacial energy (Young 1805, Dupré and Dupré 1869, Kendall 1994). When they stick to one another, soft and compliant materials such as the membrane and cytoplasm are deformed to a degree limited by their elasticity. Style, *et al.* adapted the JKR theory of contact mechanics to describe the contact surface geometry between a microscopic rigid particle and a soft substrate (Style, Hyland et al. 2013). We followed a similar approach in a simple phenomenological model expressed as the sum of mechanical strain energy ($\phi$ term) and work ($\psi$ term), respectively;

$$U \sim \phi \cdot \delta^{1+\varepsilon} - \psi \cdot \delta \; ; \tag{1}$$

Here, $U$ is the mean-field energy, $\delta$ is the invagination depth of both the membrane and cytosol (which we assume to be coupled to each other by virtue of conservation of volume of the droplet) and the exponent $\varepsilon > 0$ reflects the deformation geometry (Material and Methods) (Hertz 1882, Johnson 1971). Close to equilibrium (as $\partial U/\partial\delta$ approaches 0) we expect invagination to balance the two contributions so that $\delta^*$ minimizes energy in (1) resulting in,

$$\delta^* = \left( \frac{\psi}{\phi\,(1+\varepsilon)} \right)^{\frac{1}{\varepsilon}} \; ; \tag{2}$$

Equation (2) shows that the invagination depth $\delta$ is determined by the ratio $\psi/\phi$ and the deformation geometry $\varepsilon$. Values of $\phi$ and $\psi$ can be determined as functions of individual geometries, elasticities, and viscosities of cytosol, droplet and membrane and interfacial tensions among them (Material and Methods). These in turn can be determined by super-resolution imaging (geometries) and elastic and viscous moduli, taken from the literature or determined by active micro-rheology experiments as described next.

We used active rheology to determine the material properties of the cytosol in which cortical droplets are embedded and then, because the droplets are too small to probe directly, we calculated their properties through well-understood relationships between the properties of materials in contact and their resulting geometries, as described below. Specifically, we used optical tweezers to examine the frequency-dependent amplitude and phase responses of polystyrene beads that are embedded in cells (Fig. 3a, Material and Methods). 200 nm diameter polystyrene beads were integrated into cells by osmoporation (Fig. S9) (da Silva Pedrini, Dupont et al. 2014). Measurements of passive diffusion of the beads showed mean square displacements (MSD) close to that of random mechanical noise caused by vibration of the microscope (Fig. S9). Furthermore, we established that the osmoporation procedure did not affect rheological properties of cells by measuring the MSD of expressed viral capsid microNS particles labeled

with GFP in untreated or osmoporated cells and showing that their diffusion behaviors were identical (Fig. S10) (Munder, Midtvedt et al. 2016).

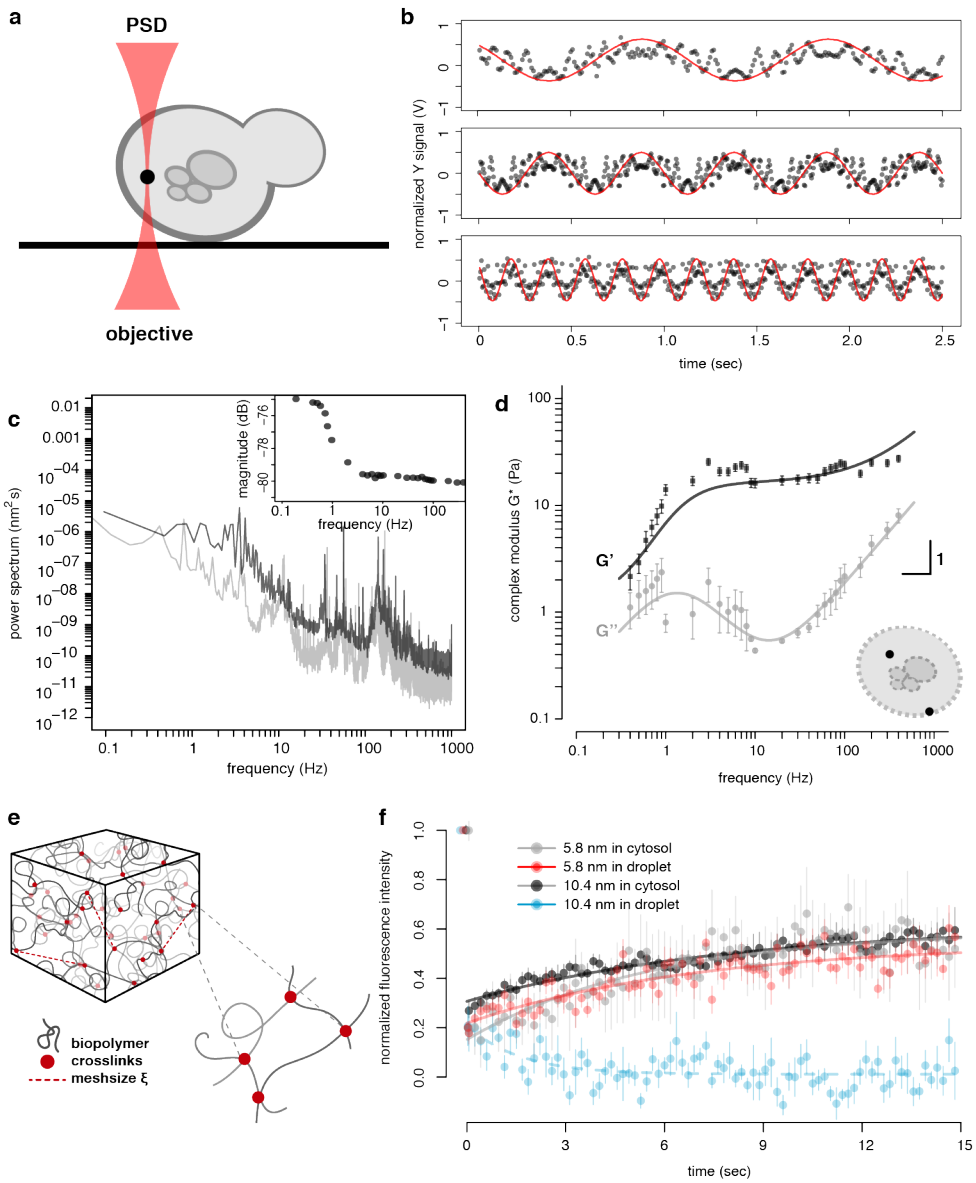


**Figure 3 | Cytosol and cortical droplets are composed of a viscoelastic amorphous network of interacting proteins** (a) We used optical tweezers (red beam between the microscope objective and a position sensitive detector (PSD) coupled to an acousto-optic device (AOD) to oscillate polystyrene beads in cells. Two pulses of osmotic shock were used to osmoporate 200 nm polystyrene beads (black) into latA-treated haploid yeast *GPD1*Δ cells. (b) PSD output signal in volts (V) as a function of time for acquisitions made at 1Hz (top), 2 Hz (middle) and 5 Hz (bottom). A bead, located in the cell periphery, was oscillated with the AOD in the Y-axis of the specimen plane with fixed tweezer movement amplitude (normalized red curve) at different frequencies. The recorded PSD raw traces (black points) were also normalized to a corresponding magnitude range (coherence cutoff of 0.9). (c) Power spectrum of the oscillated bead (black) with magnitude of response as a function of frequency (insert). (d) Decomposition

of G* as a function of frequency into G′ (storage modulus; darker squares) and G″ (loss modulus; light shade circles) for beads distributed at both the cell periphery and interior (see schematic insert; mean ± sd; n = 17) with an average trap stiffness $k_{trap}$ (mean ± se; 8.0 x $10^{-5}$ ± 2.7 x $10^{-5}$ N $m^{-1}$) and photodiode sensitivity factor $\beta$ (mean ± se; 10.7 x $10^3$ ± 2.3 x $10^3$ nm $V^{-1}$). Data was fitted to a model of an entangled and crosslinked network of flexible polymers (Material and Methods; Eq. 2.9-2.10). (e) 3D illustration and zoom-in of the latticework composed of amorphous protein chains (grey filaments) with the binding sites (red dots) through which they are non-covalently associate and the mesh size (dashed red line). (f) Fluorescence recovery after photo bleaching (FRAP) of fluorescent dye (FITC)-conjugated dextran of different size (see legend) within a Sla1-mCherry focus (red and blue) or neighbouring cytosolic regions without Sla1 signal (grey and black) in latA-treated *GPD1*Δ cells. Data points represent normalized fluorescence recovery (mean ± sd; n=3). Values for distinct dextran-FITC sizes and cell region were fitted to a single term recovery equation (Material and Methods).

For active rheology experiments, we used an acousto-optic device to oscillate the position of the optical trap in the specimen plane at frequencies over four orders of magnitude and measured the displacement of trapped beads from the trap center using back focal plane interferometry (Fig. 3b). We could thus measure the viscoelastic properties of the cytosol surrounding the beads by measuring their phase and amplitude response to the oscillations of the optical tweezers. Then by calculating the power spectrum of unforced fluctuations of the bead we obtained storage (G′) and loss (G″) moduli as a function of frequency (Fig. 3c-d, Fig. S11, Material and Methods) (Fischer, Richardson et al. 2010, Hendricks, Holzbaur et al. 2012, Hendricks and Goldman 2017).

In addition to obtaining quantities essential to calculate material properties of the cytoplasm and droplet, active rheology combined with spatiotemporal dynamics of interacting materials can inform of their structures. The mechanical properties of living cells can be compared to that of the popular children's toy "Silly Putty" (Cross 2012). Like this material, cells and underlying structures show different mechanical properties depending on the rates at which forces are applied to them (Hendricks, Holzbaur et al. 2012, Guo, Ehrlicher et al. 2013, Guo, Ehrlicher et al. 2014). Thus if a force is applied at a low velocity, the cell behaves like a viscous fluid; taking on whatever shape it is forced into. When a force is applied at higher velocity, however, the material behaves like an elastic object, bouncing back to its original shape. As we discuss below, these behaviors reflect the manner and strengths with which the molecules that make up a material interact with each other and their environment.

In specific terms, the material properties of the yeast cytoplasm and its interactions with the cortical droplet could be interpreted from the complex modulus versus frequency plot as follows (Fig. 3d): The inflection of the G' modulus at 2 Hz results in similar G' and G" values at low frequencies, which indicates that the cytosol is more viscous near rest. When deformed by the droplet growth (at a velocity of growth =2360 ± 120 nm $s^{-1}$; corresponding to a stress at ~30 ± 2 Hz) the cytosol is more elastic, whereas membrane invagination occurs at a rate at which the cytoplasm is more viscous (a velocity of 7.4 ± 2.5 nm $s^{-1}$; corresponding to 0.1 ± 0.04 Hz) (Fig. 1b, 3d, Fig. S12). The G′ and G″ we measured are similar to the cytoplasm of adherent mammalian cells and indicate that the beads are confined within a dense network of interacting

molecules (Hendricks, Holzbaur et al. 2012, Guo, Ehrlicher et al. 2013, Guo, Ehrlicher et al. 2014). We observed that the cytosol has a more malleable behavior at high frequencies than expected for an exclusively crosslinked network of flexible polymers; this may be attributed to an entangled, rather than crosslinked, network or due to compliant polymers that act more like entropic springs (Fig. 3d-e) (Koenderink, Atakhorrami et al. 2006, Lieleg, Schmoller et al. 2009, Broedersz, Depken et al. 2010, Sunthar 2010, Guo, Bourret et al. 2012, Dooling, Buck et al. 2016).

We could now determine the mechanical properties of the cortical droplet as follows. First, our micro-rheological data is consistent with both cortical droplets and cytosol behaving as elastic materials at rates above 1 Hz (Fig. 3d). Classic Hertz theory relates contact geometries of elastic materials to their mechanical properties. We could thus, use the geometry of the cortical droplets determined in our super-resolution imaging experiments and elasticity of the cytosol in which they are embedded to estimate the cortical droplet elastic modulus as 59 Pa (Fig. 1b, 3d, Material and Methods; Eq. 3.7-3.10) (Hertz 1882). These results suggest that the cortical droplets have similar material properties as the surrounding cytosol, which as an elastic (or Young's) modulus of 45 Pa at 1 Hz (Material and Methods). We estimated the mesh size of the cortical droplets by probing them with fluorophore-conjugated dextran molecules of 2.4, 5.8, and 10.4 nm in size and measured FRAP and colocalization of dextrans with Sla1-mCherry puncta (Fig. 3g-h, Fig. S13, 14). Both 2.4 nm and 5.8 nm dextran-FITC recovered equally in the Sla1 droplet and cytosolic zones, with a mobile fraction of $0.37 \pm 0.1$ and recovery rate constant of $12.7 \pm 1.1$ s. In contrast, the 10.4 nm dextran-FITC molecules cannot be replaced once the PLD-rich protein network in the droplet is formed whereas they recover in the neighbour cytosol. These results are consistent with an exclusion zone for ribosomes as discussed above and with exclusion of dextrans of 5.8 nm and more by known protein-RNA phase separated droplets called P bodies (Updike, Hachey et al. 2011, Kukulski, Schorb et al. 2012).

**Cortical droplet binding to cytosol provides energy to drive membrane invagination**

The deformation of the membrane in response to contact of a soft viscoelastic object depends on the geometries and mechanical properties of the object and the vessel it is in (in our case the cytosol of a cell) and the membrane (Fig. 4a). From all electron and super-resolution fluorescence microscopic evidence, we know that the favored geometry of the membrane is flat with invagination centered in the middle of the droplet (Fig. 4a, lower). Such geometries could be explained by a local radial stress-gradient generated by the droplet adhesion to both the membrane and cytosol. Simply stated, as the droplet grows the binding to the cytosol draws it inward and the membrane follows, mediated by its own binding to the droplet and the requirement that the volume of the droplet be conserved.

We could now quantify the work performed by the droplet to invaginate the membrane using the storage and loss moduli obtained from the micro-rheology experiments, geometric data obtained from super-resolution imaging and other data available from the literature, to solve the explicit form of the $\phi$ and $\psi$ terms (mechanical strain and work, respectively) in Equation (1) as functions of membrane and cytosol invagination $\delta$ (Material and Methods; Eq. 4.25-4.26). We first estimated with the Young-Laplace equation an interfacial tension for the droplet-cytosol interface, $\gamma_{dc}$, of $7 \times 10^{-5}$ N•m$^{-1}$, from the pressure difference across the cytosolic interface and the droplet mean curvature (Material and Methods; Eq. 4.6). This value falls within the range of $10^{-5}$ N•m$^{-1}$ to $10^{-4}$ N•m$^{-1}$ that has been reported for other protein droplets, including nucleoli and P granules (Materials and Methods; Eq. 4.9) (Brangwynne, Mitchison et al. 2011, Elbaum-Garfinkle, Kim et al. 2015).

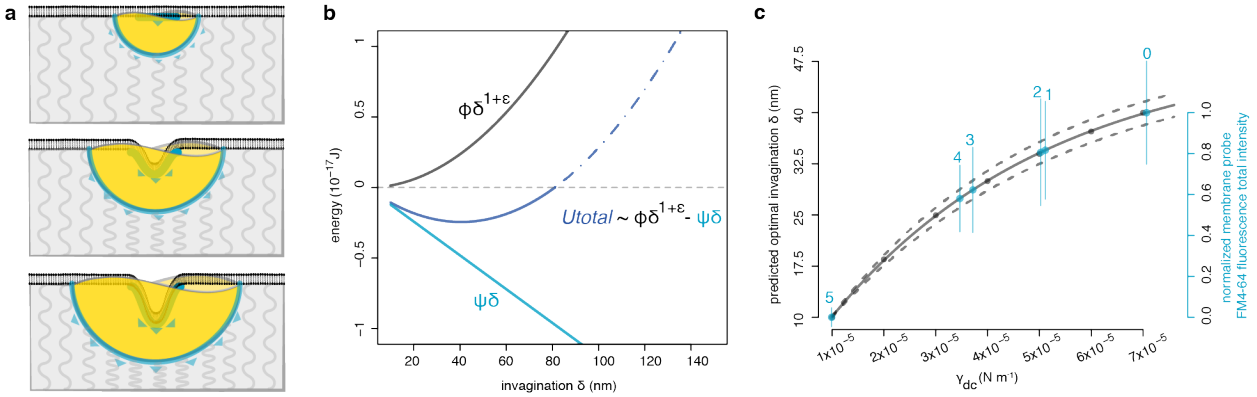


**Figure 4 | Cortical droplets do mechanical work to deform the membrane and cytosol** (a) Illustration of a cortical droplet (gold) that binds to (wets) a bilayer membrane (black) and drives membrane invagination (top to bottom). Resultant membrane deformations reflect how forces balance under a Young-Dupré adhesion gradient (blue lines and arrows). Resistance to deformation is represented by grey curved lines. (b) Equation (1) (insert) was used to calculate the energy penalties ($\phi$) and contributions ($\psi$) at the cytosol and membrane interfaces with the cortical droplet. Total energy of the system (dark blue), energy penalties (black) and energy contributions (light blue) are presented as a function of membrane invagination ($\delta$). The energy of membrane invagination is favourable for $\delta$ between about 15-80 nm (solid blue line) and unfavourable above 80 nm (dashed blue line). Quantities used to calculate energies are detailed in Figure S15 and Tables S3-S4. (c) Our model predicts that vesicle size is proportional to the strength of droplet intermolecular protein-protein interactions that are proportional to $\gamma_{dc}$, the droplet-to-cytosol interfacial tension. Predicted membrane invagination $\delta$ as a function of $\gamma_{dc}$ (left axis and black points). Data points were fitted to an exponential decay function (full line) with 95% confidence interval (dashed lines). Titration of 1,6-hexanediol was used to reduce intermolecular cohesion and therefore $\gamma_{dc}$ resulting in reduced vesicle size as measured by uptake of the lipophilic membrane probe FM4-64 into cells (Right axis, red) *versus* % HD (blue numbers, n= 25, mean ± sd) expressed as a function of the droplet-cytosol interfacial tension $\gamma_{dc}$ (Material and Methods).

With estimates of $\gamma_{dc}$ we also determined the work of adhesion that is released when the droplet surfaces are created, as described by the Young-Dupré equation (Materials and Methods; Eq.

368 4.11). Again, we assumed a radial adhesion gradient around the invagination peak in the middle
369 of the cortical droplet (Fig. 4a). We calculated an adhesion energy ($\psi$) of $4.9 \times 10^{-18}$ J from
370 interactions between the cortical droplet and both the membrane and cytosol (Fig. 4b, Fig. S15,
371 Materials and Methods; Eq. 4.26). Our results suggest that the most significant contribution of
372 the mechanical energy comes from the droplet-cytosol interface, where the adhesion energy of
373 $2.9 \times 10^{-18}$ J is enough to overcome energy penalty of $2.4 \times 10^{-18}$ J to deform both membrane and
374 cytosol. This energy cost includes the elastic, viscous, and interfacial stress penalties (Fig. 4b,
375 Fig. S15, Table S4). We also calculated an average adhesion energy of 1.3 kJ•mol$^{-1}$ at the
376 droplet-cytosol interface (Material and Methods), which is consistent with the free energies
377 expected of non-covalent interactions (Mahadevi and Sastry 2016).
378
379 Our model provides a physical framework to explain how cortical droplets do the mechanical
380 work needed to induce invagination of membranes in CME. The interface between droplets,
381 formed, by phase separation of disordered proteins into cortical bodies, and the cytosol-
382 membrane interface deforms the surrounding materials through adhesive interactions.
383 Invagination occurs when $\psi$ dominates $\phi$ and this is favored within the observed $\delta$ interval of 40
384 nm to 80 nm (Fig. S15). Notably, this predicted $\delta$ interval is within the range of plasma
385 membrane invagination of ~70 nm at which point a membrane scission mechanism is activated
386 and vesicle generation is completed (Idrissi, Blasco et al. 2012).
387
388 We propose that cortical droplets store and dissipate mechanical energy in the form of surface
389 tension, whereby the composition of the droplets determines their interfacial interactions and
390 provides the energy for adhesion and invagination of membranes. Accordingly, the underlying
391 energy stored within the droplets and the balance of interactions amongst droplet components
392 and solvent governs the nature of the interface. The potential energy $\psi$ of droplets, which by the
393 work-energy theorem should be equivalent to the total work of adhesion, should be dictated by
394 the density and strengths of physical interactions amongst proteins within the droplet (the droplet
395 cohesion and interfacial tensions). We tested this assumption by weakening the favorable free
396 energies of the protein-protein interactions that hold droplet components together using 1,6-
397 hexanediol (HD). These are the interactions that drive the phase separation of cortical droplets,
398 and so would correspond to a decrease of the droplet surface tension ($\gamma_{dc}$ or $\psi$). Our model
399 predicts that invagination depth should continuously vary with $\psi$ from Equation (2). We titrated
400 HD below the effective concentration that prevents protein phase separation and quantified
401 individual membrane excision events by quantifying uptake of the lipophilic membrane probe
402 FM4-64 into cells by fluorescence microscopy (Fig. 2a, Material and Methods). In LatA treated
403 *GPD1*Δ cells, this measures the amount of labeled membrane taken up into cells under the action
404 of cortical droplets alone. By increasing subcritical HD concentration (corresponding to a
405 decrease in $\psi$), the average fluorescence-labeled membrane per vesicle (a proxy for invagination
406 $\delta$) was continuously reduced over one order of magnitude in the value of $\gamma_{dc}$ (Fig. 4c, Material
407 and Methods; Eq. 2.8). This observation fits with the reduced membrane invagination that we

408 predicted at the outset (*i.e.*, that δ scales with the ψ/ϕ ratio) when the droplet cohesion ($\gamma_{dc}$ or ψ)
409 is also reduced (Fig. 4c, Material and Methods; Eq. 4.2).
410

411 ## Discussion

412

413 Our results provide a framework for answering many questions regarding CME and other
414 membrane budding processes. Given our observations, how is CME coupled to multiple
415 signaling pathways that integrate to regulate vesicle formation? For instance, the PLD-containing
416 CME proteins we investigated are enriched for multiple phosphorylation sites, which undergo
417 changes in response to activation of a CME-regulating signaling pathway (Kanshin, Bergeron-
418 Sandoval et al. 2015). Since the amount and distribution of charge in disordered regions of
419 proteins regulate their interactions and conformations (Das and Pappu 2013), such post-
420 translational modifications may be important to regulating CME. Our fluorescence microscopy
421 and electron micrographic evidence from the literature suggests that the cortical droplet remains
422 associated temporarily with mature vesicles (Kukulski, Schorb et al. 2012). Does the droplet play
423 any role in trafficking and fusing with, for instance, plasma membrane (protein recycling) or
424 lysosome (protein degradation)? CME underlies several fundamental mechanisms of vesicle
425 trafficking and attendant membrane and vesicle protein cargo transport, including late secretory
426 pathways, endocytosis and neuronal synaptic vesicle recycling. Yeast and human proteins
427 implicated in clathrin-mediated vesicle trafficking are enriched for long disordered protein
428 domains (47/23% of proteins with long consecutive disordered regions of 30 residues and more
429 for humans and yeast, respectively) whereas those involved in two other vesicle trafficking
430 systems are not (COPI: 8/5%; COPII: 8/5%) (Pietrosemoli, Pancsa et al. 2013, Busch, Houser et
431 al. 2015). These observations argue for investigating the generality and conservation of protein
432 droplet adhesion-driven membrane invagination as the basis of clathrin-mediated vesicle
433 trafficking in the absence of actin polymerization.

434

435 It is possible that other liquid-liquid phase separated protein and protein nucleic acid droplets
436 may influence cellular sub-structural dynamics and shape thus contributing to cell, tissue, and
437 organism morphology (Bergeron-Sandoval, Safaee et al. 2016). More broadly, interfacial contact
438 potentials between different biological materials could represent a vastly underestimated source
439 of complex pattern formation in biology, such as has been observed in embryonic tissue layers
440 (Foty, Pfleger et al. 1996) or recently in a model of growing brain convolutions (Tallinen, Chung
441 et al. 2016) or in protein stabilization (Gupta, Donlan et al. 2017).

442

443

## Acknowledgments

The authors acknowledge support from CIHR grants MOP-GMX-152556 (SWM) and the US National Institutes of Health grant R01NS056114 (RVP). We thank Simon Alberti for insightful discussions and microNS plasmid, Jackie Vogel for strains, Jacqueline Kowarzyk for technical assistance, Susan Liebman for the Sup35 plasmids, Daniel Zenklussen and Pascal Raymond for help with FRAP experiments.

## Author contributions

L.P.S.B. and S.W.M. designed all of the research and R.V.P. helped in designing part of the research; L.P.S.B. performed biological research; L.P.S.B. and H.K.H. performed micro rheology experiments; L.P.B.S., H.K.H., A.J.E. and A.G.H analyzed micro rheology data; L.P.S.B., A.J.E. and S.W.M. analyzed biological data; L.P.B.S., H.K.H. and P.F. developed physical droplet model; L.P.S.B., R.V.P., and S.W.M. combined physical models with data analysis; all authors wrote the paper.

## Supplementary Materials

Materials and Methods

Figures S1-S15

Tables S1-S4

Movies S1

References

## References

1. Aghamohammadzadeh, S. and K. R. Ayscough (2009). "Differential requirements for actin during yeast and mammalian endocytosis." Nat Cell Biol 11 (8): 1039-1042.
2. Alberti, S., R. Halfmann, O. King, A. Kapila and S. Lindquist (2009). "A systematic survey identifies prions and illuminates sequence features of prionogenic proteins." Cell 137 (1): 146-158.
3. Avinoam, O., M. Schorb, C. J. Beese, J. A. Briggs and M. Kaksonen (2015). "ENDOCYTOSIS. Endocytic sites mature by continuous bending and remodeling of the clathrin coat." Science 348 (6241): 1369-1372.
4. Banjade, S., Q. Wu, A. Mittal, W. B. Peeples, R. V. Pappu and M. K. Rosen (2015). "Conserved interdomain linker promotes phase separation of the multivalent adaptor protein Nck." Proc Natl Acad Sci U S A 112 (47): E6426-6435.
5. Bergeron-Sandoval, L. P., N. Safaee and S. W. Michnick (2016). "Mechanisms and Consequences of Macromolecular Phase Separation." Cell 165 (5): 1067-1079.
6. Boettner, D. R., J. L. D'Agostino, O. T. Torres, K. Daugherty-Clarke, A. Uygur, A. Reider, B. Wendland, S. K. Lemmon and B. L. Goode (2009). "The F-BAR protein Syp1 negatively

483 regulates WASp-Arp2/3 complex activity during endocytic patch formation." Curr Biol 19 (23):
484 1979-1987.
485 7. Boulant, S., C. Kural, J. C. Zeeh, F. Ubelmann and T. Kirchhausen (2011). "Actin dynamics
486 counteract membrane tension during clathrin-mediated endocytosis." Nat Cell Biol 13 (9): 1124-
487 1131.
488 8. Brach, T., C. Godlee, I. Moeller-Hansen, D. Boeke and M. Kaksonen (2014). "The initiation of
489 clathrin-mediated endocytosis is mechanistically highly flexible." Curr Biol 24 (5): 548-554.
490 9. Brangwynne, C. P., C. R. Eckmann, D. S. Courson, A. Rybarska, C. Hoege, J. Gharakhani, F.
491 Julicher and A. A. Hyman (2009). "Germline P granules are liquid droplets that localize by
492 controlled dissolution/condensation." Science 324 (5935): 1729-1732.
493 10. Brangwynne, C. P., T. J. Mitchison and A. A. Hyman (2011). "Active liquid-like behavior of
494 nucleoli determines their size and shape in Xenopus laevis oocytes." Proc Natl Acad Sci U S A
495 108 (11): 4334-4339.
496 11. Broedersz, C. P., M. Depken, N. Y. Yao, M. R. Pollak, D. A. Weitz and F. C. MacKintosh
497 (2010). "Cross-link-governed dynamics of biopolymer networks." Phys Rev Lett 105 (23):
498 238101.
499 12. Busch, D. J., J. R. Houser, C. C. Hayden, M. B. Sherman, E. M. Lafer and J. C. Stachowiak
500 (2015). "Intrinsically disordered proteins drive membrane curvature." Nat Commun 6: 7875.
501 13. Carlsson, A. E. and P. V. Bayly (2014). "Force generation by endocytic actin patches in budding
502 yeast." Biophys J 106 (8): 1596-1606.
503 14. Crick, S. L., K. M. Ruff, K. Garai, C. Frieden and R. V. Pappu (2013). "Unmasking the roles of
504 N-and C-terminal flanking sequences from exon 1 of huntingtin as modulators of polyglutamine
505 aggregation." Proceedings of the National Academy of Sciences 110 (50): 20075-20080.
506 15. Cross, R. (2012). "Elastic and viscous properties of Silly Putty." American Journal of Physics 80:
507 870-875.
508 16. da Silva Pedrini, M. R., S. Dupont, A. de Anchieta Camara, Jr., L. Beney and P. Gervais (2014).
509 "Osmoporation: a simple way to internalize hydrophilic molecules into yeast." Appl Microbiol
510 Biotechnol 98 (3): 1271-1280.
511 17. Darwin, C. (1859). On the origin of species by means of natural selection, or, The preservation of
512 favoured races in the struggle for life. London, J. Murray.
513 18. Das, R. K. and R. V. Pappu (2013). "Conformations of intrinsically disordered proteins are
514 influenced by linear sequence distributions of oppositely charged residues." Proc Natl Acad Sci U
515 S A 110 (33): 13392-13397.
516 19. Dmitrieff, S. and F. Nedelec (2015). "Membrane Mechanics of Endocytosis in Cells with
517 Turgor." PLoS Comput Biol 11 (10): e1004538.
518 20. Dooling, L. J., M. E. Buck, W. B. Zhang and D. A. Tirrell (2016). "Programming Molecular
519 Association and Viscoelastic Behavior in Protein Networks." Adv Mater 28 (23): 4651-4657.
520 21. Drubin, D. G., M. Kaksonen, C. Toret and Y. Sun (2005). "Cytoskeletal networks and pathways
521 involved in endocytosis." Novartis Found Symp 269: 35-42; discussion 43-36, 223-230.
522 22. Dupré, A. and P. Dupré (1869). Théorie mécanique de la chaleur Gauthier-Villars.
523 23. Elbaum-Garfinkle, S., Y. Kim, K. Szczepaniak, C. C. Chen, C. R. Eckmann, S. Myong and C. P.
524 Brangwynne (2015). "The disordered P granule protein LAF-1 drives phase separation into
525 droplets with tunable viscosity and dynamics." Proc Natl Acad Sci U S A 112 (23): 7189-7194.
526 24. Ewers, H., W. Romer, A. E. Smith, K. Bacia, S. Dmitrieff, W. Chai, R. Mancini, J. Kartenbeck,
527 V. Chambon, L. Berland, A. Oppenheim, G. Schwarzmann, T. Feizi, P. Schwille, P. Sens, A.
528 Helenius and L. Johannes (2010). "GM1 structure determines SV40-induced membrane
529 invagination and infection." Nat Cell Biol 12 (1): 11-18; sup pp 11-12.
530 25. Feric, M., N. Vaidya, T. S. Harmon, D. M. Mitrea, L. Zhu, T. M. Richardson, R. W. Kriwacki, R.
531 V. Pappu and C. P. Brangwynne (2016). "Coexisting Liquid Phases Underlie Nucleolar
532 Subcompartments." Cell 165 (7): 1686-1697.
533 26. Fischer, M., A. C. Richardson, S. N. Reihani, L. B. Oddershede and K. Berg-Sorensen (2010).

"Active-passive calibration of optical tweezers in viscoelastic media." Rev Sci Instrum 81 (1): 015103.
27. Foty, R. A., C. M. Pfleger, G. Forgacs and M. S. Steinberg (1996). "Surface tensions of embryonic tissues predict their mutual envelopment behavior." Development 122 (5): 1611-1620.
28. Godlee, C. and M. Kaksonen (2013). "Review series: From uncertain beginnings: initiation mechanisms of clathrin-mediated endocytosis." J Cell Biol 203 (5): 717-725.
29. Guilak, F., J. R. Tedrow and R. Burgkart (2000). "Viscoelastic properties of the cell nucleus." Biochem Biophys Res Commun 269 (3): 781-786.
30. Guo, H., G. Bourret, R. B. Lennox, M. Sutton, J. L. Harden and R. L. Leheny (2012). "Entanglement-controlled subdiffusion of nanoparticles within concentrated polymer solutions." Phys Rev Lett 109 (5): 055901.
31. Guo, M., A. J. Ehrlicher, M. H. Jensen, M. Renz, J. R. Moore, R. D. Goldman, J. Lippincott-Schwartz, F. C. Mackintosh and D. A. Weitz (2014). "Probing the stochastic, motor-driven properties of the cytoplasm using force spectrum microscopy." Cell 158 (4): 822-832.
32. Guo, M., A. J. Ehrlicher, S. Mahammad, H. Fabich, M. H. Jensen, J. R. Moore, J. J. Fredberg, R. D. Goldman and D. A. Weitz (2013). "The role of vimentin intermediate filaments in cortical and cytoplasmic mechanics." Biophys J 105 (7): 1562-1568.
33. Gupta, K., J. A. Donlan, J. T. Hopper, P. Uzdavinys, M. Landreh, W. B. Struwe, D. Drew, A. J. Baldwin, P. J. Stansfeld and C. V. Robinson (2017). "The role of interfacial lipids in stabilizing membrane protein oligomers." Nature 541 (7637): 421-424.
34. Harold, F. M. (1990). "To shape a cell: an inquiry into the causes of morphogenesis of microorganisms." Microbiol Rev 54 (4): 381-431.
35. Haviv, L., D. Gillo, F. Backouche and A. Bernheim-Groswasser (2008). "A cytoskeletal demolition worker: myosin II acts as an actin depolymerization agent." J Mol Biol 375 (2): 325-330.
36. Hendricks, A. G. and Y. E. Goldman (2017). "Measuring Molecular Forces Using Calibrated Optical Tweezers in Living Cells." Methods Mol Biol 1486: 537-552.
37. Hendricks, A. G., E. L. Holzbaur and Y. E. Goldman (2012). "Force measurements on cargoes in living cells reveal collective dynamics of microtubule motors." Proc Natl Acad Sci U S A 109 (45): 18447-18452.
38. Hertz, H. R. (1882). Ueber die Beruehrung elastischer Koerper (On Contact Between Elastic Bodies). Leipzig, Germany, 1895.
39. Hom, R. A., M. Vora, M. Regner, O. M. Subach, W. Cho, V. V. Verkhusha, R. V. Stahelin and T. G. Kutateladze (2007). "pH-dependent binding of the Epsin ENTH domain and the AP180 ANTH domain to PI (4,5)P2-containing bilayers." J Mol Biol 373 (2): 412-423.
40. Hyman, A. A., C. A. Weber and F. Julicher (2014). "Liquid-liquid phase separation in biology." Annu Rev Cell Dev Biol 30: 39-58.
41. Idrissi, F. Z., A. Blasco, A. Espinal and M. I. Geli (2012). "Ultrastructural dynamics of proteins involved in endocytic budding." Proc Natl Acad Sci U S A 109 (39): E2587-2594.
42. Idrissi, F. Z., H. Grotsch, I. M. Fernandez-Golbano, C. Presciatto-Baschong, H. Riezman and M. I. Geli (2008). "Distinct acto/myosin-I structures associate with endocytic profiles at the plasma membrane." J Cell Biol 180 (6): 1219-1232.
43. Jiang, H., S. Wang, Y. Huang, X. He, H. Cui, X. Zhu and Y. Zheng (2015). "Phase transition of spindle-associated protein regulate spindle apparatus assembly." Cell 163 (1): 108-122.
44. Johnson, K. L. K., K.;Roberts, A. D. (1971). "Surface energy and the contact of elastic solid." Proc. R. Soc. Lond. A. 324: 301-313.
45. Kaksonen, M., C. P. Toret and D. G. Drubin (2005). "A modular design for the clathrin- and actin-mediated endocytosis machinery." Cell 123 (2): 305-320.
46. Kanshin, E., L. P. Bergeron-Sandoval, S. S. Isik, P. Thibault and S. W. Michnick (2015). "A cell-signaling network temporally resolves specific versus promiscuous phosphorylation." Cell Rep 10 (7): 1202-1214.

47. Kendall, K. (1994). "Adhesion: molecules and mechanics." Science 263 (5154): 1720-1725.
48. Khurana, R., C. Coleman, C. Ionescu-Zanetti, S. A. Carter, V. Krishna, R. K. Grover, R. Roy and S. Singh (2005). "Mechanism of thioflavin T binding to amyloid fibrils." J Struct Biol 151 (3): 229-238.
49. Koenderink, G. H., M. Atakhorrami, F. C. MacKintosh and C. F. Schmidt (2006). "High-frequency stress relaxation in semiflexible polymer solutions and networks." Phys Rev Lett 96 (13): 138307.
50. Kroschwald, S., S. Maharana, D. Mateju, L. Malinovska, E. Nuske, I. Poser, D. Richter and S. Alberti (2015). "Promiscuous interactions and protein disaggregases determine the material state of stress-inducible RNP granules." Elife 4: e06807.
51. Kukulski, W., A. Picco, T. Specht, J. A. Briggs and M. Kaksonen (2016). "Clathrin modulates vesicle scission, but not invagination shape, in yeast endocytosis." Elife 5.
52. Kukulski, W., M. Schorb, M. Kaksonen and J. A. Briggs (2012). "Plasma membrane reshaping during endocytosis is revealed by time-resolved electron tomography." Cell 150 (3): 508-520.
53. Li, D., L. Shao, B. C. Chen, X. Zhang, M. Zhang and B. Moses (2015). "Extended-resolution structured illumination imaging of endocytic and cytoskeletal dynamics." Science (New York, NY).
54. Lieleg, O., K. M. Schmoller, M. M. Claessens and A. R. Bausch (2009). "Cytoskeletal polymer networks: viscoelastic properties are determined by the microscopic interaction potential of cross-links." Biophys J 96 (11): 4725-4732.
55. Lin, Y., D. S. W. Protter, M. K. Rosen and R. Parker (2015). "Formation and Maturation of Phase-Separated Liquid Droplets by RNA-Binding Proteins." Molecular Cell 60 (2): 208-219.
56. Mahadevi, A. S. and G. N. Sastry (2016). "Cooperativity in Noncovalent Interactions." Chem Rev 116 (5): 2775-2825.
57. Malinovska, L., S. Kroschwald and S. Alberti (2013). "Protein disorder, prion propensities, and self-organizing macromolecular collectives." Biochim Biophys Acta 1834 (5): 918-931.
58. Meshcheryakov, A., E. Steudle and E. Komor (1992). "Gradients of turgor, osmotic pressure, and water potential in the cortex of the hypocotyl of growing ricinus seedlings : effects of the supply of water from the xylem and of solutes from the Phloem." Plant Physiol 98 (3): 840-852.
59. Molliex, A., J. Temirov, J. Lee, M. Coughlin, A. P. Kanagaraj, H. J. Kim, T. Mittag and J. P. Taylor (2015). "Phase separation by low complexity domains promotes stress granule assembly and drives pathological fibrillization." Cell 163 (1): 123-133.
60. Munder, M. C., D. Midtvedt, T. Franzmann, E. Nuske, O. Otto, M. Herbig, E. Ulbricht, P. Muller, A. Taubenberger, S. Maharana, L. Malinovska, D. Richter, J. Guck, V. Zaburdaev and S. Alberti (2016). "A pH-driven transition of the cytoplasm from a fluid- to a solid-like state promotes entry into dormancy." Elife 5.
61. Nott, T. J., E. Petsalaki, P. Farber, D. Jervis, E. Fussner, A. Plochowietz, T. D. Craggs, D. P. Bazett-Jones, T. Pawson, J. D. Forman-Kay and A. J. Baldwin (2015). "Phase transition of a disordered nuage protein generates environmentally responsive membraneless organelles." Mol Cell 57 (5): 936-947.
62. Pappu, R. V., X. Wang, A. Vitalis and S. L. Crick (2008). "A polymer physics perspective on driving forces and mechanisms for protein aggregation." Arch Biochem Biophys 469 (1): 132-141.
63. Picco, A., M. Mund, J. Ries, F. Nedelec and M. Kaksonen (2015). "Visualizing the functional architecture of the endocytic machinery." Elife 4.
64. Pietrosemoli, N., R. Pancsa and P. Tompa (2013). "Structural disorder provides increased adaptability for vesicle trafficking pathways." PLoS Comput Biol 9 (7): e1003144.
65. Pollard, T. D. and J. A. Cooper (2009). "Actin, a central player in cell shape and movement." Science 326 (5957): 1208-1212.
66. Rog, O., S. Kohler and A. F. Dernburg (2017). "The synaptonemal complex has liquid crystalline properties and spatially regulates meiotic recombination factors." Elife 6.

636 67. Scher-Zagier, J. K. and A. E. Carlsson (2016). "Local Turgor Pressure Reduction via Channel
637 Clustering." Biophys J 111 (12): 2747-2756.
638 68. Style, R. W., C. Hyland, R. Boltyanskiy, J. S. Wettlaufer and E. R. Dufresne (2013). "Surface
639 tension and contact with soft elastic solids." Nat Commun 4: 2728.
640 69. Sunthar, P. (2010). Polymer Rheology, Springer New York.
641 70. Tallinen, T., J. Chung, F. Rousseau, N. Girard, J. Lefèvre and L. Mahadevan (2016). "On the
642 growth and form of cortical convolutions." Nature Physics 12: 588–593.
643 71. Thompson, D. A. W. (1917). On growth and form. Cambridge Eng., University press.
644 72. Toombs, J. A., B. R. McCarty and E. D. Ross (2009). "Compositional Determinants of Prion
645 Formation in Yeast." Molecular and Cellular Biology 30 (1): 319-332.
646 73. Updike, D. L., S. J. Hachey, J. Kreher and S. Strome (2011). "P granules extend the nuclear pore
647 complex environment in the C. elegans germ line." J Cell Biol 192 (6): 939-948.
648 74. Watson, H. A., M. J. Cope, A. C. Groen, D. G. Drubin and B. Wendland (2001). "In vivo role for
649 actin-regulating kinases in endocytosis and yeast epsin phosphorylation." Mol Biol Cell 12 (11):
650 3668-3679.
651 75. Wheeler, J. R., T. Matheny, S. Jain, R. Abrisch and R. Parker (2016). "Distinct stages in stress
652 granule assembly and disassembly." Elife 5.
653 76. Young, T. (1805). "An essay on the cohesion of fluids." Philosophical Transactions of the Royal
654 Society of London 95: 65-87.
655 77. Zhang, H., S. Elbaum-Garfinkle, E. M. Langdon, N. Taylor, P. Occhipinti, A. A. Bridges, C. P.
656 Brangwynne and A. S. Gladfelter (2015). "RNA Controls PolyQ Protein Phase Transitions."
657 Molecular Cell 60 (2): 220-230.
658